中国科学技术大学
University of Science and Technology of China

Dust Attenuation and Metallicity for Star-Forming Galaxies in MaNGA Survey

PhD. Thesis Defense

Berzaf Berhane Teklu

Supervisor: Prof. Xu Kong

Department: Astronomy

October 31, 2019

Overview

1. Dust Attenuation Curve for Local Subgalactic Star-forming Regions

2. The Local Star Formation Rate Surface Density and Metallicity Relation for Star-Forming Galaxies

Introduction

- Extinction: individual sight-lines, absorption + scattering out of the line-of-sight, related to the size distribution and composition of the dust grains
- Attenuation: extended sources, extinction + scattering back into the line-of-sight, a strong dependence on the dust geometry

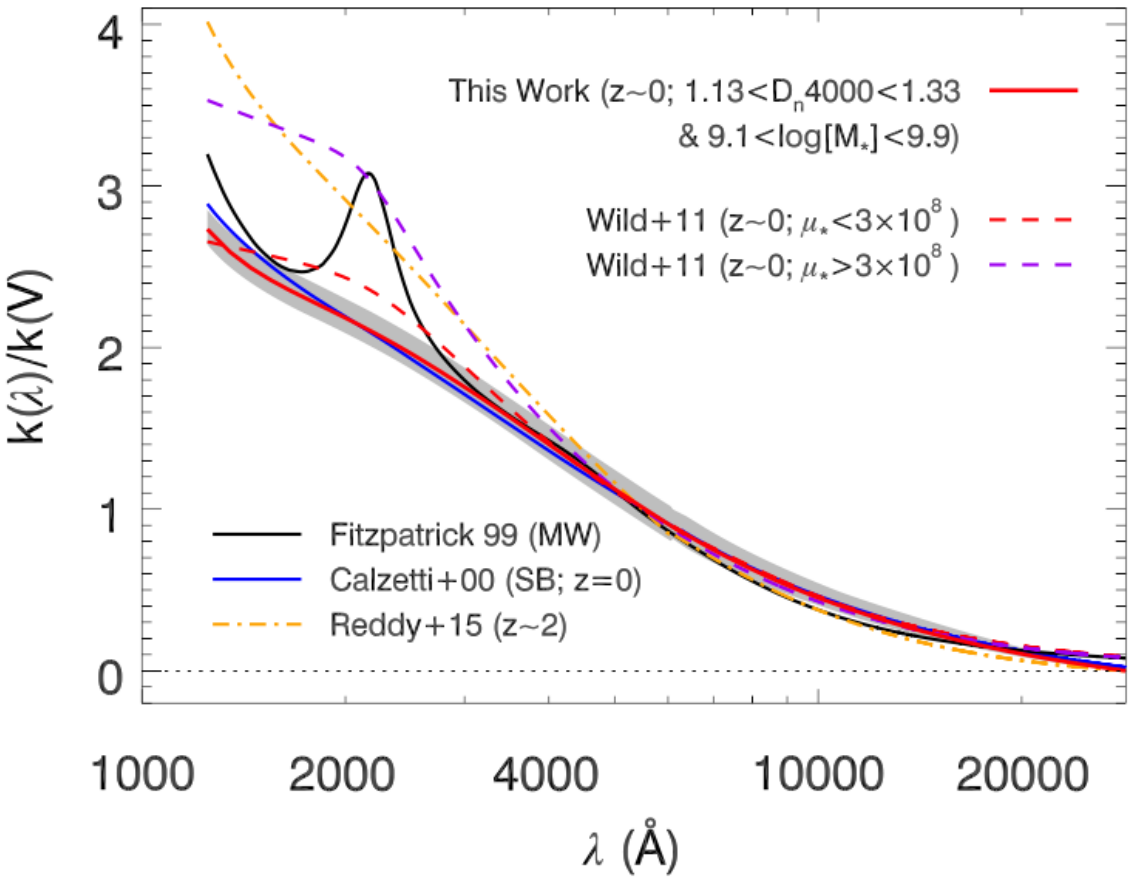

- In local universe, average attenuation curves determined for both SB (Calzetti et al. 1994, 2000) and normal SFGs(Wild et al. 2011; Battisti et al. 2016; Battisti et al. 2017b).

- Difficulties: SED–due to the unknown and complex intrinsic SED
  - only the average attenuation curve can be derived.
  - previous works were derived based on photometry/spectra of either the entire galaxies or the most central regions
  - our knowledge to the wavelength-dependence of dust attenuation at the scale of H II region is very limited.
- Therefore, it is important to determine an average attenuation curve for sub-galactic regions.
- examine whether the curves vary with physical scale or local physical properties.

Data

MaNGA Survey

- Target: 10,000 galaxies
- Wavelength: 3600Å-10300Å, $0.01 < z < 0.14$
- In this work, we take the MaNGA data from the SDSS DR14 (Abolfathi et al. 2018)
- The parent sample, 2812 datacubes.

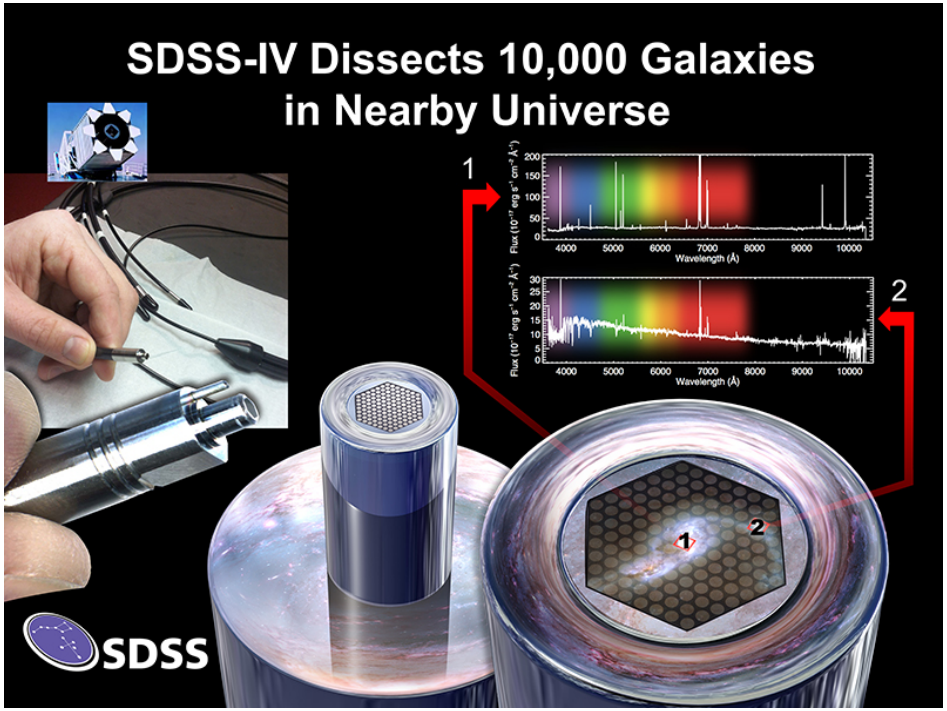

Spectral Fitting and Emission-line Measurements

- First correct the Galactic foreground extinction based on the color excesses.
- continua of spectra are fitted via the public full-spectrum fitting code of STARLIGHT.
- During the fitting
  - A dust attenuation curve of Calzetti et al. (2000) and spectrum templates from the Bruzual & Charlot (2003) models are adopted
- To obtain the pure emission line spectra, best-fit continua are then subtracted from the original spectra

contin .....

- Each emission line is fitted with single Gaussian profile utilizing the MPFIT IDL code.
- The signal-to-noise ratios (S/N) of emission lines are estimated following the procedure of Ly et al. (2014).
- we use the Balmer decrement to correct the galactic internal reddening,
  - Assuming an intrinsic flux ratio of Hα/H$\beta = 2.86$ under the Case B recombination

Physical Parameters

- M_* and b/a are extracted from the NSA catalog.
- Following the method of Barrera-Ballesteros et al. (2016), we generate Σ_*.
- Divide each spaxel Σ_* from the output of STARLIGHT fits by its corresponding physical area.
- We use the dust-corrected Hα emission-line luminosity to determine the SFR for each spaxel, using the relation from Kennicutt et al. 1998:

$$\mathrm{SFR}(\mathrm{M}_\odot \mathrm{yr}^{-1}) = 4.4 \times 10^{-42} \times \mathrm{L}(\mathrm{H}\alpha)(\mathrm{erg\ s}^{-1}). \quad (1)$$

Sample Selection

- we first select SFGs based on the criterion of $\mathrm{NUV} - r < 4$
- Only spaxels with S/N(Hα), S/N(Hβ), ([O III]λ5007) are > 5, ([N II]λ6583) > 3, and the S/N of continua > 10 are used.
- The SF regions can be classified by BPT diagram.
- sample of 326, 000 spaxels from 1227 SFGs.

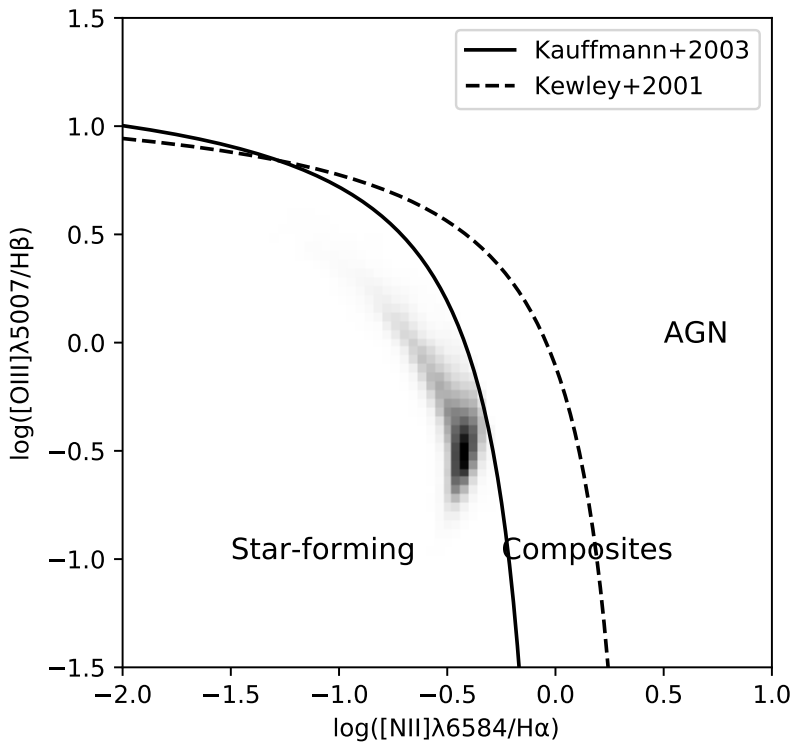

Method

Galaxies with similar morphology, similar SFHs but different inclinations, and thus different dust attenuation, the reddening law can be derived from the comparison of their spectra.

This method begins with three main assumptions as following:

1. The dust attenuation is dominated by a foreground-like dust component.
2. The reddening of ionized gas is correlated with that of the stellar continuum.
3. Galaxies/regions have roughly similar SFHs and stellar populations.

The first assumption gives the relation between the observed and intrinsic fluxes as

$$f_{\lambda,\mathrm{obs}} = f_{\lambda,\mathrm{int}} e^{-\tau_\lambda}, \tag{2}$$

$$\tau_\mathrm{B} = \tau_{\mathrm{H}\alpha} - \tau_{\mathrm{H}\beta} = \ln\left(\frac{f_{\mathrm{H}\alpha,\mathrm{obs}}/f_{\mathrm{H}\beta,\mathrm{obs}}}{2.86}\right), \tag{3}$$

$$E(B-V)_\mathrm{gas} = \frac{1.086\tau_\mathrm{B}}{k_{\mathrm{H}\beta} - k_{\mathrm{H}\alpha}}, \tag{4}$$

- The second assumptions allows us to use nebular attenuation derived from the Balmer decrement to trace the stellar attenuation.
- Use τ_B to represent the relative reddening of stellar continuum.

Selective attenuation

Considering two H II regions with the same SFHs and thus very similar intrinsic spectra, denoting these two spectra as $f_{\lambda,i}$ and $f_{\lambda,j}$, their relative optical depth is

$$\tau_{i,j}(\lambda) = -\ln \frac{f_{\lambda,i}}{f_{\lambda,j}}. \tag{5}$$

Then the selective attenuation can be determined from

$$Q_{i,j}(\lambda) = \frac{\tau_{i,j}(\lambda)}{\delta\tau_{\mathrm{B},i,j}}, \tag{6}$$

i.e., $\delta\tau_{\mathrm{B},i,j} = \tau_{\mathrm{B},i} - \tau_{\mathrm{B},j}$.

contin .....

Then the total-to-selective extinction can be expressed as $k(\lambda) = fQ_{i,j}(\lambda) + R_V$.

- The factor f describes the difference between dust attenuation of ionized gas and stars.

Therefore, the basic steps of this strategy are

1. select spectra that meet the third assumption;
2. divide them into bins with different stellar reddening according to their $\tau_{\rm B}$;
3. calculate $Q_{i,j}(\lambda)$ for the average spectra of two bins with different $\tau_{\rm B}$;
4. determine f and R_V.

contin .....

Due to the complication of galactic SFH, the third assumption needed with additional age criterion.

- use $D_n(4000)$ as age indicator to select spaxels with similar ages due to its positive correlation with age.
- The evolution of $D_n(4000)$ depends strongly on metallicity when age $> 10^9$ yr.

To reduce the effect of metallicity,

- spaxels with $1.1 \leq D_n(4000) < 1.3$ and divide them into two $D_n(4000)$ bins with a width of $\Delta D_n(4000) = 0.1$
- final sample 157,000 spaxels from 982 SFGs.

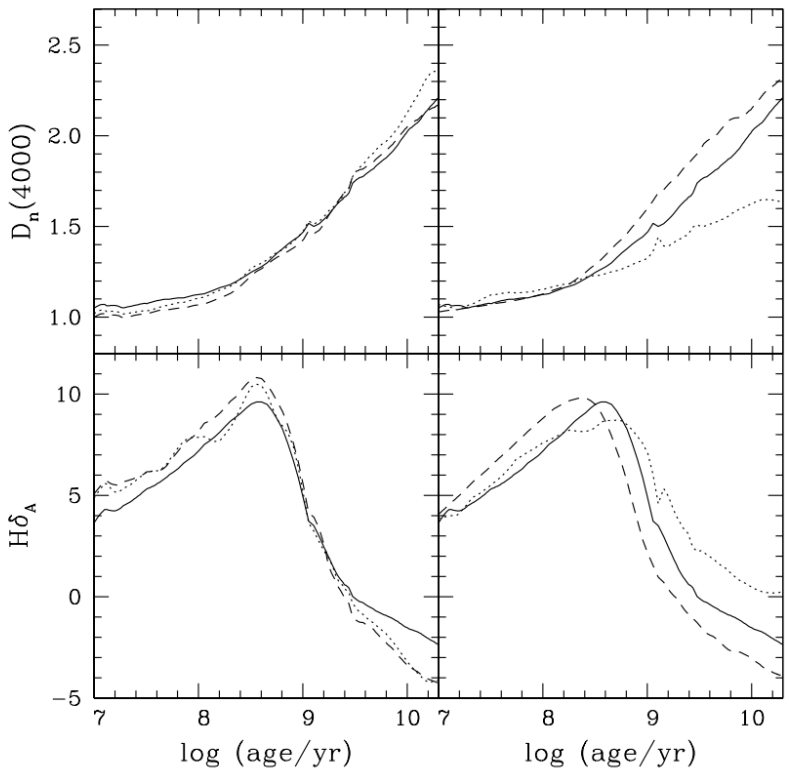

contin .....

Utilizing the Gaussian fitting results,

- subtract emission lines from the de-redshifted spectra to create emission line-free spectra
- which are then smoothed in a wavelength window of 100 Å.
- The smoothed spectra are normalized to their rest-frame flux densities at $\lambda = 5500$ Å.
- Within each $D_n(4000)$ bin, we divide spaxels into $\tau_{\rm B}$ bins with a step of $\Delta\tau_{\rm B} = 0.1$.
- An average spectrum is obtained for spaxels within the same $\tau_{\rm B}$ bin, and is taken as the template spectrum of the bin.

Result: Average flux density of galaxies

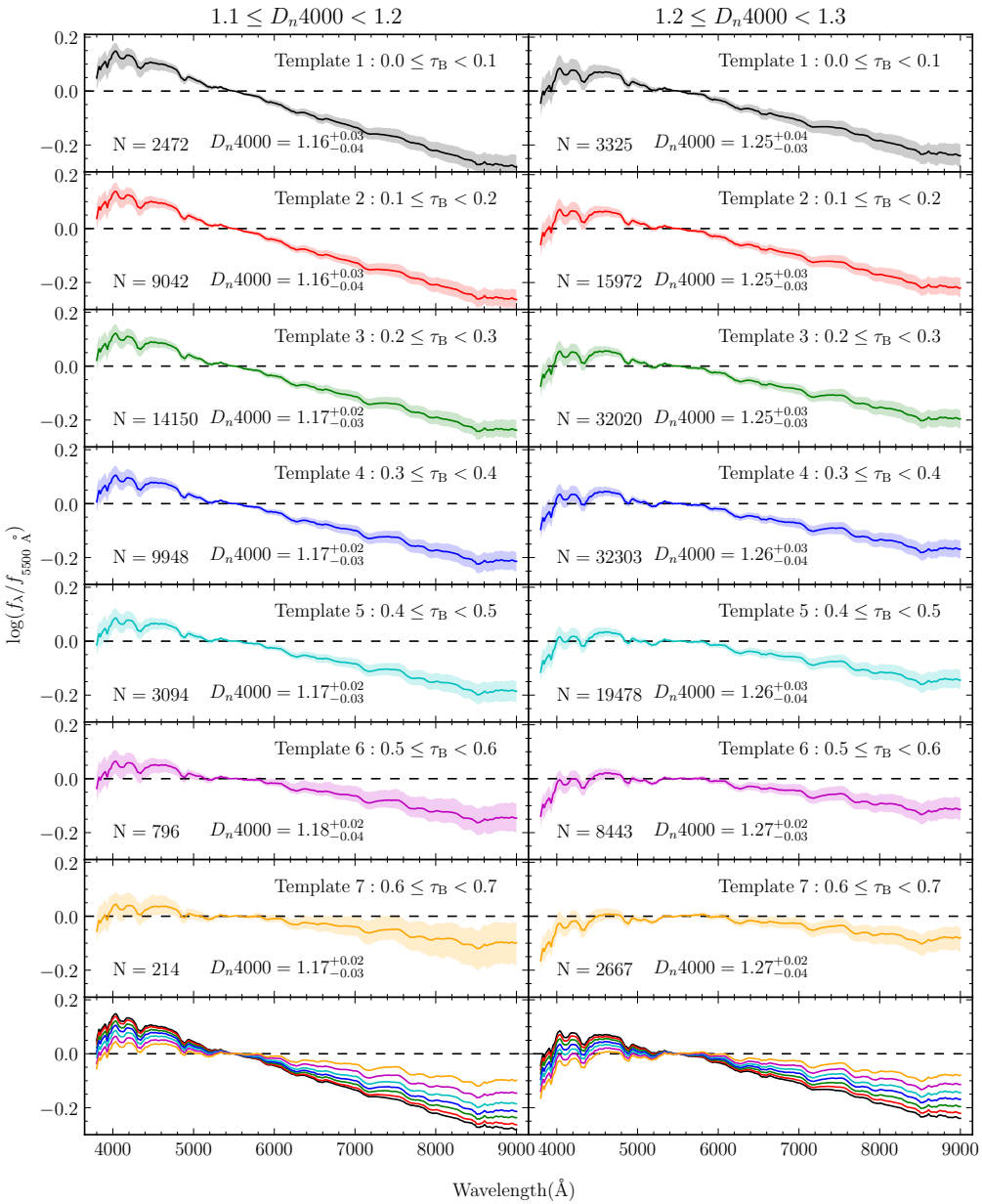

- Average spectra in different τ_B bins
- a clear trend that the shape of templates becomes flatter as the increases τ_B ,
- indicating a higher dust reddening of the stellar continua.

Attenuation Curve of All Spaxels

- $Q_{\rm eff}(\lambda)$, is calculated by averaging all the selective attenuation curve $Q_{i,j}(\lambda)$
- fitted with a third-order polynomial

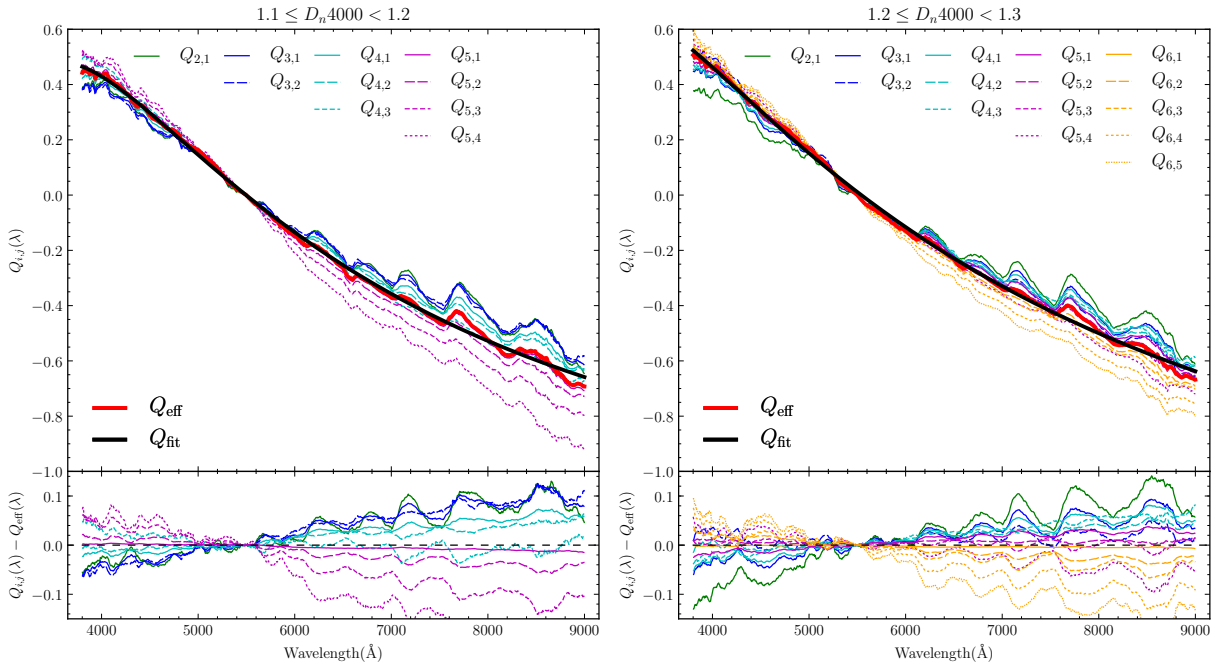

$Q_{i,j}(\lambda)$ derived from all adopted template spectra

$$Q_{\rm fit}(x) = p_0 + p_1 x + p_2 x^2 + p_3 x^3, \tag{7}$$

where $x = 1/\lambda$, and λ is in units of Å. The best-fit results within the wavelength range of 3800–9000 Å are

$$Q_{\rm fit}(\lambda) = -1.3448 + 0.1151x + 0.6238x^2 - 0.1544x^3, \tag{8}$$

$$Q_{\rm fit}(\lambda) = -1.7998 + 1.0351x + 0.0596x^2 - 0.0447x^3, \tag{9}$$

$k(\lambda) = fQ(\lambda) + R_V$. By definition, $k(B) - k(V) \equiv 1$. The factor f can be derived from

$$f = \frac{1}{Q_{\rm fit}(B) - Q_{\rm fit}(V)}. \tag{10}$$

The wavelength of B and V bands to be 4400 Å and 5500 Å

Comparison between attenuation curves

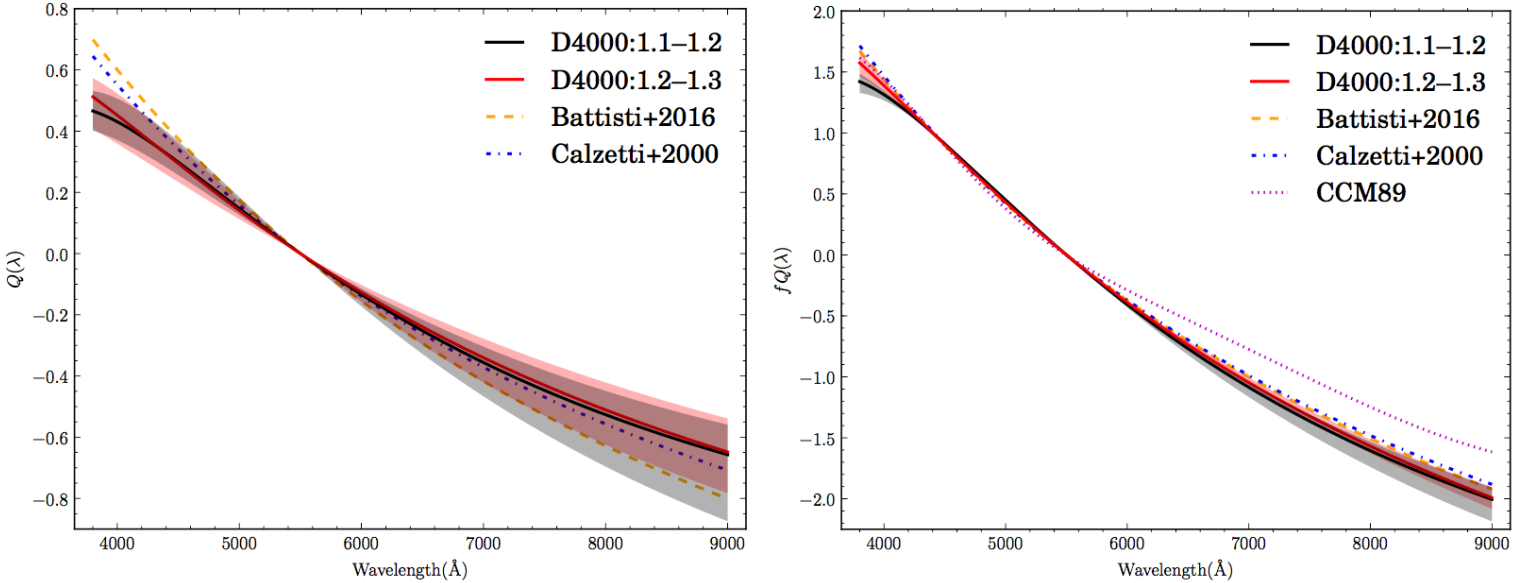

- Both $Q_{\rm fit}(\lambda)$ and $fQ_{\rm fit}(\lambda)$ for the two $D_n(4000)$ subsamples are consistent with each other
- indicating that the shape of attenuation curve is independent of $D_n(4000)$ within the wavelength range
- roughly consistent with those of Calzetti et al. 2000 and Battisti al et. 2016 at $\lambda > 4400$ Å, regardless of the $D_n(4000)$ ranges

Dependence on Local Physical Properties

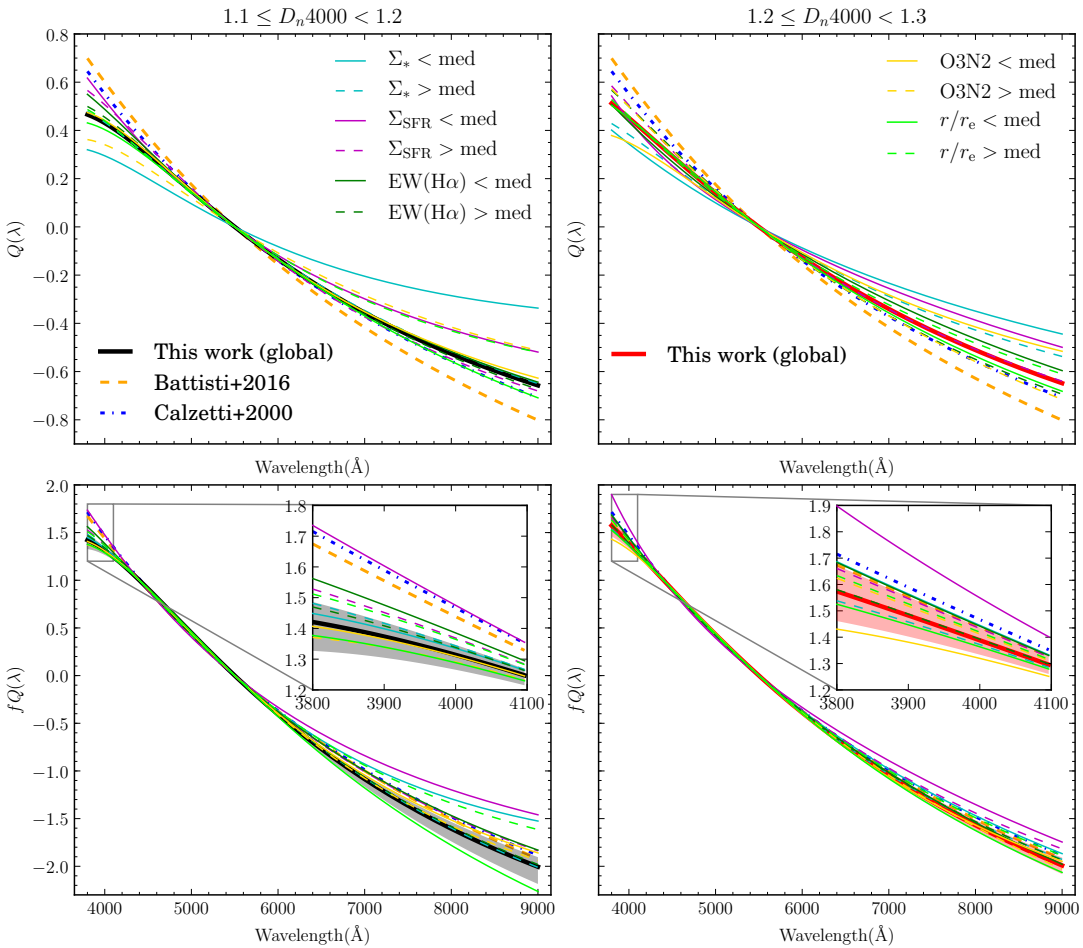

1. $1.1 \leq D_n(4000) < 1.2$,
   - $\Sigma_* <$ med and $\Sigma_{\rm SFR} <$ med large deviations from the global
   - flatter curve, H II regions at the low-mass end of the SGMS
2. $1.2 \leq D_n(4000) < 1.3$,
   - the variations in $fQ(\lambda)$ is smaller.
   - each local physical property, consistent with each other in $fQ(\lambda)$

contin .....

For the binning in $r/r_{\rm e}$ also gives significant difference in the $fQ(\lambda)$ for $1.1 \leq D_n(4000) < 1.2$.

- the inner regions of galaxies have a steeper and outer regions a much flatter
- However, this difference vanishes for the $1.2 \leq D_n(4000) < 1.3$ subsample.
- Given the similar behavior of Σ_* and $\Sigma_{\rm SFR}$ to $r/r_{\rm e}$ in $fQ(\lambda)$
- Argue that these two surface densities might be such more intrinsic properties.
- The differences in Σ_* and $\Sigma_{\rm SFR}$ can explain the observed different slopes of the curve between the inner and outer bins.

contin .....

- Different sSFR or Z share similar average selective attenuation curve.
- For the younger subsample ($1.1 \leq D_n(4000) < 1.2$)
  - H II regions with smaller Σ_*, smaller $\Sigma_{\rm SFR}$, or larger $r/r_{\rm e}$
  - Tend to have a flatter attenuation curves compared to the global and two reference curves
- For slightly older stellar population, no evident difference is observed between the binned results for all local properties we explored.
- different size distribution of dust grains or dust/star geometry between the younger and slightly older H II regions.

Dependence on Global Physical Properties

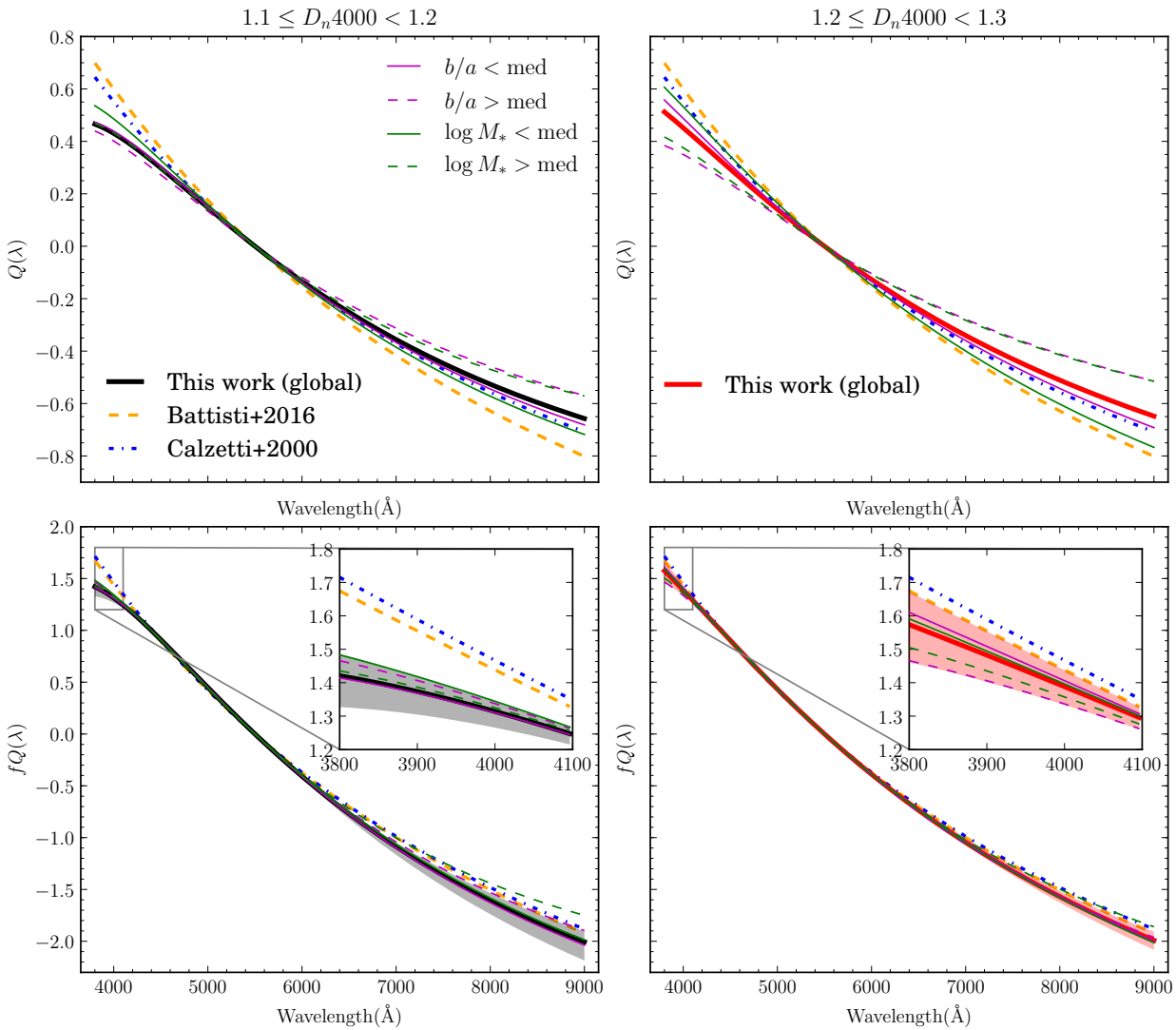

- $fQ(\lambda)$ of the more massive galaxies is flatter than less massive galaxies for the younger population.
- For the older population, the shape shows no dependence on M_*.

SUMMARY

The average attenuation curve of subgalactic H II regions shows no dependence on $D_n(4000)$ within $1.1 \leq D_n(4000) < 1.3$, and is similar to the one derived from either SB or normal SFGs.

For the younger population, spaxels at the low-mass end of the SGMS or resided in the outer regions of the host galaxies tend to have flatter attenuation curves compared to the global ones.

For the older population, no dependence on local physical properties is found for the average attenuation curves.

For $1.1 \leq D_n(4000) < 1.2$, H II regions resided in more massive galaxies tend to have shallower attenuation curve, while the slope of attenuation curve seems to be unaffected by the inclination.

Introduction

A tight correlation b/n the stellar mass and the metallicity of galaxies: as stellar mass increases, the metallicity increases.

- SFR appears to be a second parameter of MZR at z=0
- anti-correlation is noticeable in M10 at low masses but nearly vanishes at high masses

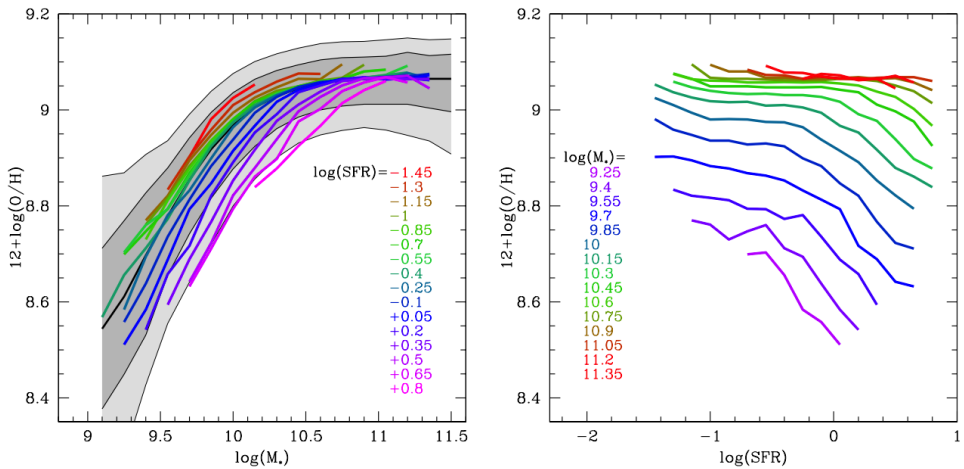

Mannucci et al. (2010)

- Yates et al. (2012) shows that the metallicity increases, rather than decreases, with increasing SFR for massive galaxies.
- Some studies could not confirm the secondary relation of SFR
- These discrepancies may largely arise from the use of different metallicity indicators or different galaxy selection criteria adopted in different studies.

Sample Selection

- we first select SFGs based on the criterion of $\mathrm{NUV} - r < 4$
- Only spaxels with S/N(Hα) > 5, S/N(Hβ) > 5, S/N([O III]λ5007) > 5, S/N([N II]λ6583) > 3, and with continuum S/N > 3 and EW(Hα) > 10 Å.
- The spaxels can be classified by BPT diagram.
- spaxels affected by the AGN are excluded by applying the Kauffmann et al. (2003) demarcation.
- sample of about 740000 spaxels from 1120 SFGs.

Determinations of Metallicity

1. The N2O2 index: The calibrated metallicity using the relation in Kewley & Dopita (2002) is given by

$$12 + \log(\mathrm{O/H}) = \log(1.54020 + 1.26602 \times \mathrm{N2O2} + 0.167977 \times \mathrm{N2O2}^2) + 8.93, \tag{11}$$

2. O3N2 index: The diagnostic of O3N2 index (Alloin et al. 1979) is characterized by

$$12 + \log(\mathrm{O/H}) = 8.505 - 0.221 \times \mathrm{O3N2} \tag{12}$$

3. N2 index: N2 calibrated metallicity is determined by Marino et al. 2013 and expressed as

$$12 + \log(\mathrm{O/H}) = 8.667 + 0.455 \times \mathrm{N2}. \tag{13}$$

4. N2S2 index: This diagnostic established by Dopita et al. (2016)

$$12 + \log(\mathrm{O/H}) = 8.77 + \mathrm{N2S2} + 0.264 \times \mathrm{N2}. \tag{14}$$

Result: Dependence of the $\Sigma_* - Z$ and $\Sigma_{\rm SFR}$

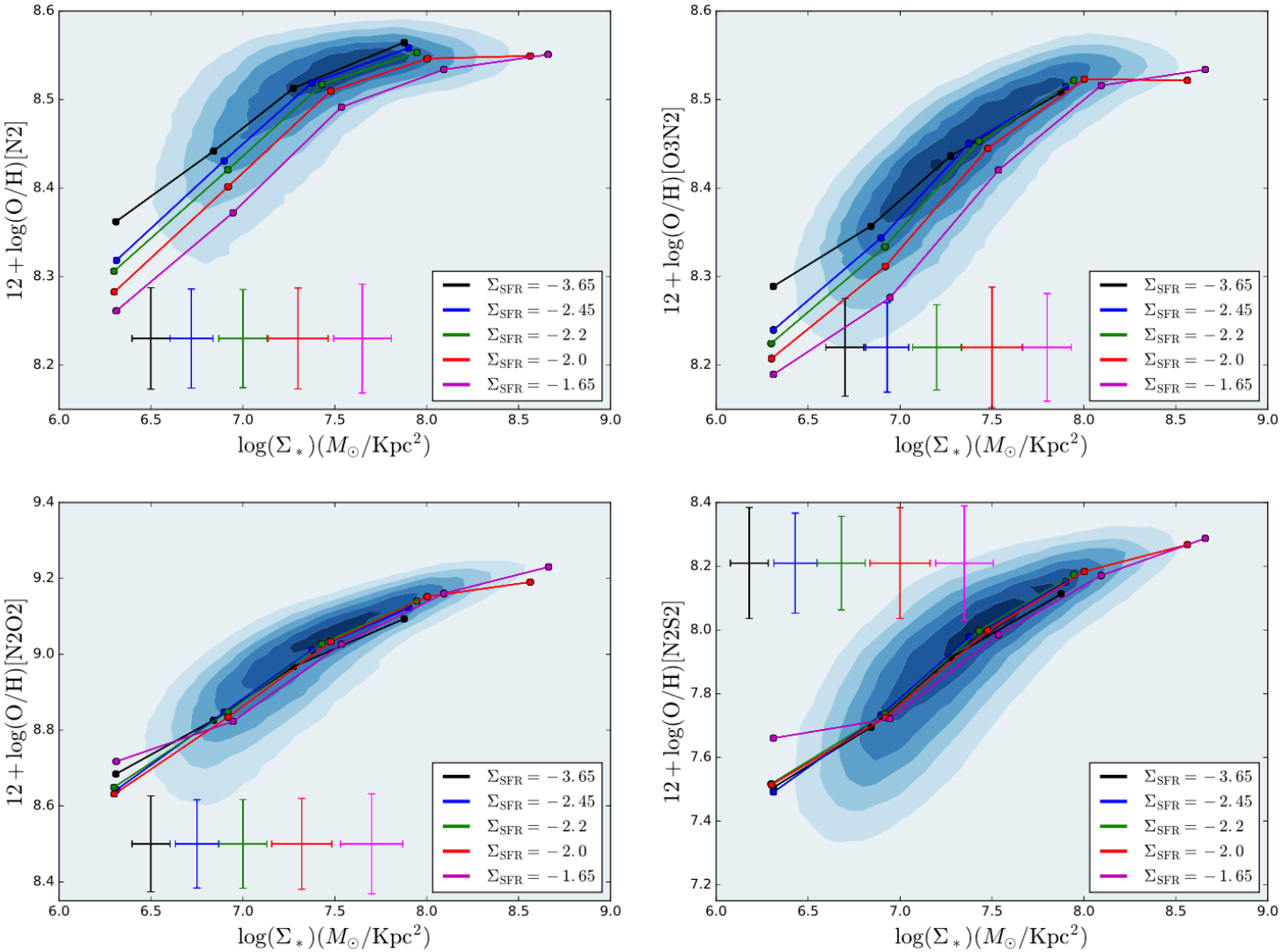

$\Sigma_{\rm SFR}$ – Z Relation on M_*

The x-axis - $\Sigma_{\rm SFR}$ and y-axis - the metallicity of N2, O3N2, N2O2 & N2S2.

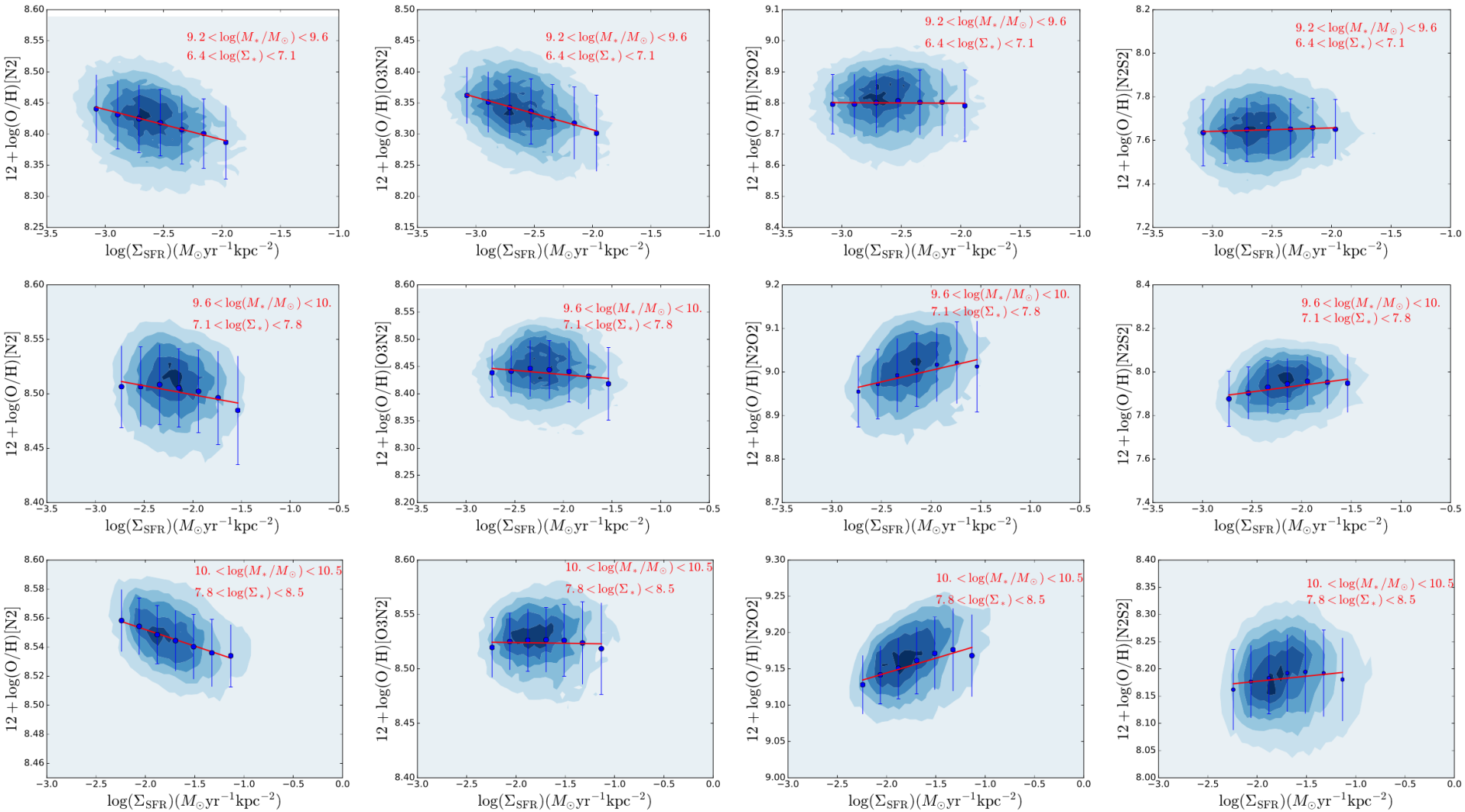

For low mass bin subsamples,

- Find a clear and strong anti-correlation between $\Sigma_{\rm SFR}$ and Z
- with $r = -0.33$ and $r = -0.38$, for metallicity index N2 and O3N2, respectively.
- However, for N2O2 and N2S2 metallicity indices, no correlation is found at this mass range.
- relations indicate for higher (lower) stellar mass bins, the correlation is weak (strong) for $\Sigma_{\rm SFR} - Z$.
- for O3N2 metallicity, at higher stellar mass ($M_* > 10.$), we find a flatter trend, which is similar to the flatten of MZR at high masses.

The mixed results on this $\Sigma_{\rm SFR} - Z$ relations are possibly caused by different metallicity estimation, which has systematic errors on calibration, and the calculation of $\Sigma_{\rm SFR}$ from strong emission line.

Dependence of [O III]λ5007/[O II]λ3727 on Metallicity

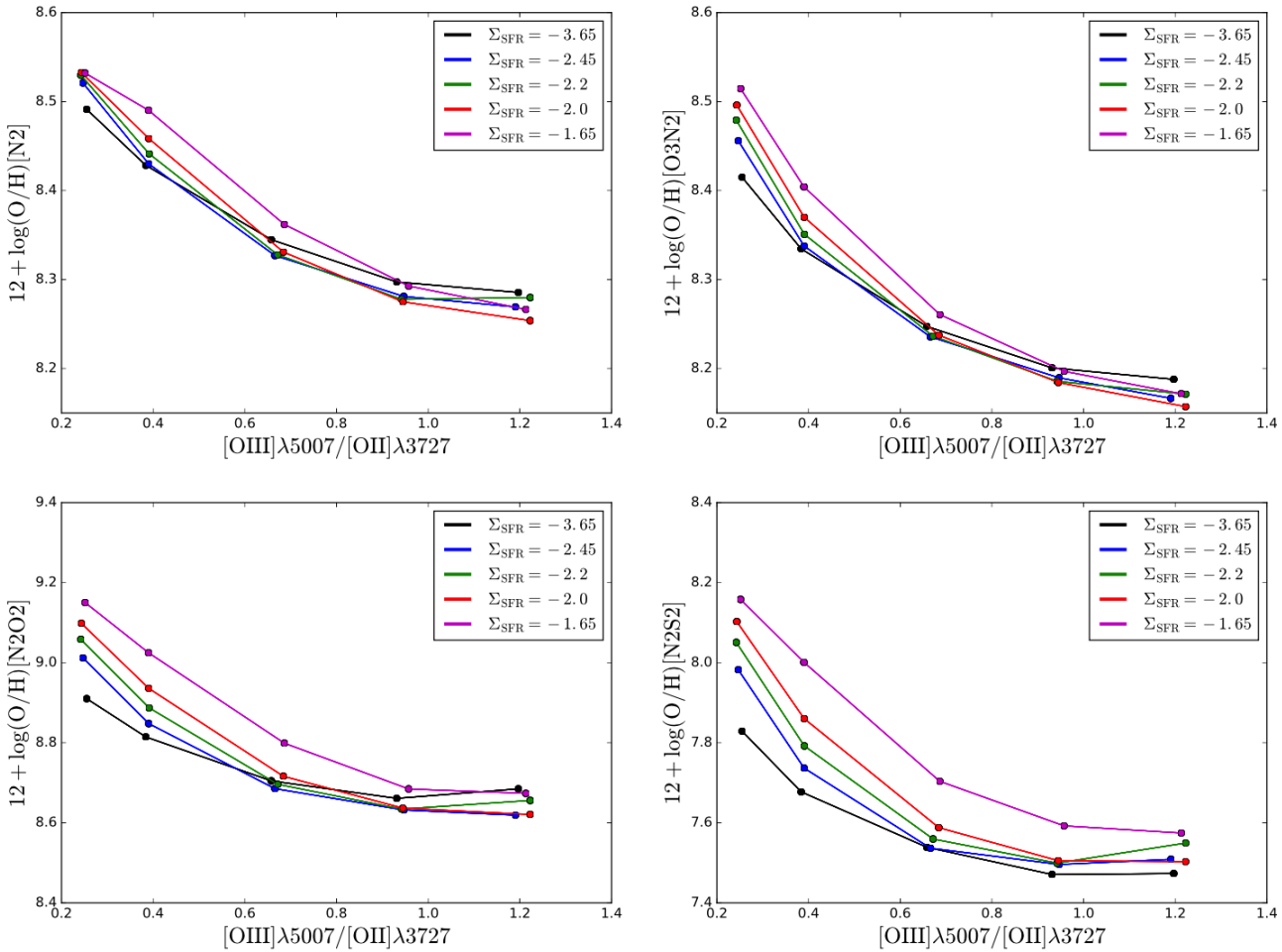

- the metallicity decreases with the increasing of O32 ratio
- At a fixed ratio of O32, the Z increases with the increasing of $\Sigma_{\rm SFR}$.

The Fundamental Metallicity Relation

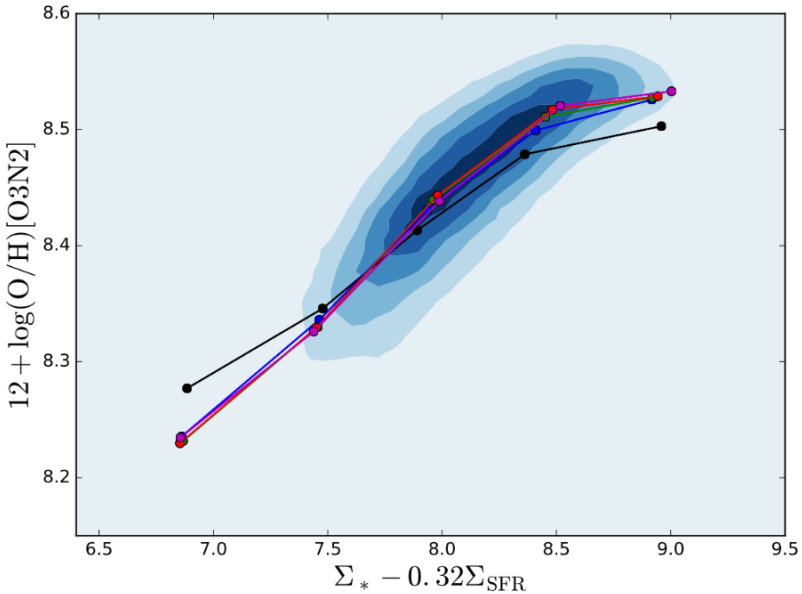

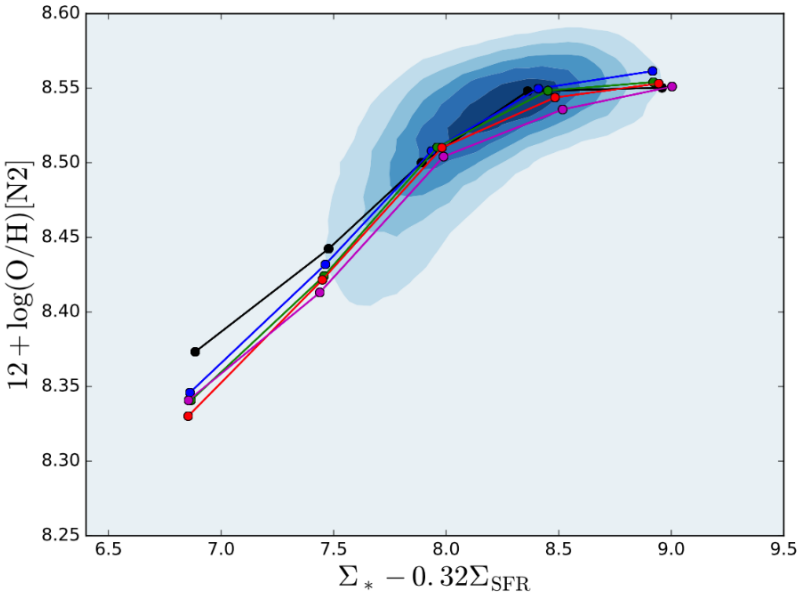

$$\mu_\alpha = log\Sigma_* - \alpha log\Sigma_{\mathrm{SFR}}$$

- setting $log(M_*/M_\odot) > 9.6$, and $\alpha = 0.32$ as proposed by Mannucci et al. 2010 that reduce the scatter of our sample.
- find the scatters of our sample are $\sigma = 0.28$ dex and 0.26 dex using metallicity N2 and O3N2

Discussion
Physical Explanation of O32 Ratio and Local Metallicity

The ionization parameter and O32 ratio commonly demonstrate dependence on metallicity since the ionizing spectrum related to metallicity.

- low-metallicity stars generate higher ionizing photons
- and have a harder ionizing spectrum as that of an anti-correlation with metallicity and ionization parameter.
- hardness of the ionizing spectrum increases with decreasing metallicity

The FMR and $\Sigma_{\rm SFR} - Z$

Using the metallicity calibration N2 and O3N2, there is an

- anti-correlation between Z and $\Sigma_{\rm SFR}$, N2 and O3N2
- A positive correlation at the high mass range, N2O2 and N2S2 indexes.
- Yates et al. 2012, SFR anti-correlates to metallicity at lower stellar masses, then the relation inverts to a positive correlation at higher stellar masses.
- They argue that the inversion is the consequence of gas-rich mergers at higher stellar masses fueling a starburst.

Different metallicity calibrations give different correlations between the $\Sigma_{\rm SFR}$ or Z and Σ_*.

- These results imply that the emission line fluxes of our samples may affect the $\Sigma_{\rm SFR}$
- or are caused by the ionization parameter.
- the strong correlation between the ratio of O32 and the local metallicity, this is known as the ionization parameter is sensitive to oxygen abundance.
- Determination of metallicity using strong emission lines may bias the ionization parameter.

Our result is partly consistent with a reported negative correlation between metallicity and SFR (Mannucci et al 2010, Andrews et al. 2013), and at the higher mass bins, the positive correlation is also in agreement with Kashino et al. 2016.

SUMMARY

We find a strong correlation with local $\Sigma_{\rm SFR}$ using O3N2, N2, but the trend is not obvious with N2O2 and N2S2.

We find a mixed relation of $\Sigma_{\rm SFR}$ – Z (anti-correlation/positive correlation) at lower/higher stellar mass bins according to metallicity derivation.

The dependence of the ratio of O32 on metallicity, a higher ionization parameter is found at lower metallicity, and the lower ionization parameter tends to higher metallicity.

The FMR after exclusion of low stellar mass, projection of local Σ_*, Z, and $\Sigma_{\rm SFR}$, and find that the scatters are reduced when using N2, O3N2, comparing to Σ_* – Z.

Publications

- Dust Attenuation Curve For Local Subgalactic Star-Forming Regions; **Berzaf Berhane Teklu**, Ze-Sen Lin, Xu Kong, Enci Wang, Yulong Gao, Ning Hu, Hai-Yang Liu and Qing Liu; Submitted to ApJ
- The Local Metallicity and Star Formation Rate Surface Density Relation for Star-Forming Galaxies; **Berzaf Berhane Teklu**,Yulong Gao, Xu Kong, Ze-Sen Lin, Zhixiong Liang, Submitted to ApJ
- What Determines the Local Metallicity of Galaxies: Global Stellar Mass, Local Stellar Mass Surface Density, or Star Formation Rate; Yulong Gao, Enci Wang, Xu Kong, Zesen Lin, Guilin Liu, Haiyang Liu, Qing Liu, Ning Hu, **Berzaf Berhane Teklu**, Xinkai Chen, and Qinyuan Zhao; The ApJ, 868:89
- Elevation or Suppression? The Resolved Star Formation Main Sequence of Galaxies with Two Different Assembly Modes;Qing Liu, Enci Wang, Zesen Lin, Yulong Gao, Haiyang Liu, **Berzaf Berhane Teklu**, and Xu Kong; The ApJ, 857:17


THANK YOU!!!
谢谢！
ያመሰግናሉ!